THE JOURNAL OF PHYSICAL CHEMISTRY C

Article

Cite This: J. Phys. Chem. C 2018, 122, 15929−15936

pubs.acs.org/JPCC

Pressure Impact on the Crystal Structure, Optical, and Transport Properties in Layered Oxychalcogenides BiCu*Ch*O (*Ch* = S, Se)

Qian Zhang,[†] Chen Chen,[‡] Nana Li,[†] Quan Huang,[†] Yu He,[†,&] Xuqiang Liu,[†,§] Bihan Wang,[†] Dongzhou Zhang,[£] Duck Young Kim,[†] Yonggang Wang,[*,†] Bo Xu,[‡] and Wenge Yang[*,†,¥]

[†]Center for High Pressure Science and Technology Advanced Research (HPSTAR), Shanghai 201203, China

[‡]State Key Laboratory of Metastable Materials Science and Technology, Yanshan University, Qinhuangdao, Hebei 066004, China

[&]Key Laboratory of High-Temperature and High-Pressure Study of the Earth's Interior, Institute of Geochemistry, Chinese Academy of Sciences, Guiyang, Guizhou 550081, China

[§]School of Material Science and Engineering, Northeastern University, Shenyang 110819, China

[£]Hawaii Institute of Geophysics & Planetology, University of Hawaii Manoa, Honolulu, Hawaii 96822, United States

[¥]High Pressure Synergetic Consortium (HPSynC), Geophysical Laboratory, Carnegie Institution of Washington, Argonne, Illinois 60439, United States

Supporting Information

ABSTRACT: The layered oxychalcogenides BiCu*Ch*O (*Ch* = S, Se, Te) represent a unique family of two-dimensional semiconductors with extraordinary optoelectronic and thermoelectric properties. Chemical strategies such as elemental doping have been used to modify their crystal structures and electronic configurations for better photocatalytic performances. Herein, we report the pressure impact on the crystalline and electronic band structures of BiCu*Ch*O (*Ch* = S, Se) with in situ synchrotron X-ray diffraction, Raman spectroscopy, electric resistivity and photocurrent measurements, and first-principle calculations. Under pressure, the crystalline lattices shrink continuously without symmetry breaking, which enhances the crystal field splitting; on the other hand, the pressure-induced charge delocalization causes the band broadening. The competition between the crystal field and charge delocalization demonstrates an efficient tool for band gap engineering: the electrical conductivity is enhanced below 12 GPa and monotonically decreases up to 40 GPa. In addition, BiCuSeO exhibits considerable photocurrent up to ∼40 GPa, which suggests its potential application in pressure-responsive optoelectrical devices. The comprehensive studies of the pressure effect on the crystal structure and electronic properties in two-dimensional semiconductors provide and in-depth understanding for developing new optoelectronic materials under extreme conditions.

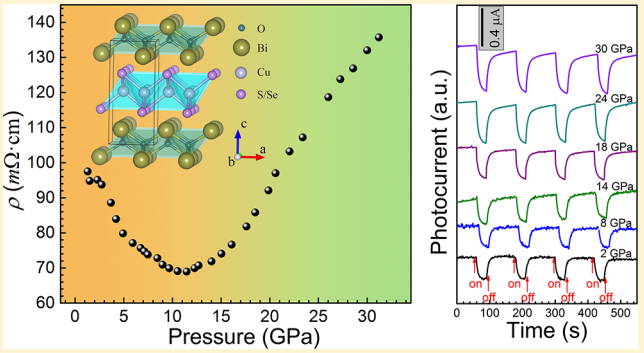

INTRODUCTION

Quaternary mixed-anion semiconductors with the general formula *Ln*M*X*O (*Ln* = trivalent rare earth cation, *M* = Ag, Fe, Cu; *X* = pnictogen or chalcogen), usually adopt the tetragonal ZrCuSiAs-type structure. Within such a two-dimensional (2D) structure, the M_2X_2 layer offers a carrier conduction path, which is sandwiched between the charge receiver Ln_2O_2 layers.[1,2] Conduction carriers are two-dimensionally confined in the M_2X_2 layers, leading to strong interactions among the electrons. Thus, those compounds established with distinct element combinations exhibit luxuriant physical properties, such as superconductivity in oxypnictides[1−3] and good optoelectronic performance in oxychalcogenides.[4,5] Among them, *Ln*Cu*Ch*O (*Ch* = chalcogen) semiconductors are frequently studied as promising transparent p-type semiconductors with wide band gaps and a good optical transmission at both the visible and near-infrared ranges.[4,6] Previous studies showed that the full substitution of trivalent lanthanide cations by Bi^{3+} in these oxychalcogenides could achieve much narrower band gaps while maintaining their crystallographic symmetry.[7] Particularly, BiCuSeO with a moderate band gap (0.8 eV) and intrinsically low thermal conductivity has attracted intensive research interest and has developed into a new promising thermoelectric (TE) material in the medium temperature range.[8,9] In the past decade, significant achievements have been gained in optimizing its TE performance through various strategies including modulation doping,[10] band structure engineering,[11,12] and microstructure regulation.[13] These chemical manipulations can boost the TE performance of BiCuSeO from the initial *ZT* value of 0.76 for

Received: May 25, 2018
Revised: June 21, 2018
Published: June 25, 2018

DOI: 10.1021/acs.jpcc.8b04996
J. Phys. Chem. C 2018, 122, 15929−15936

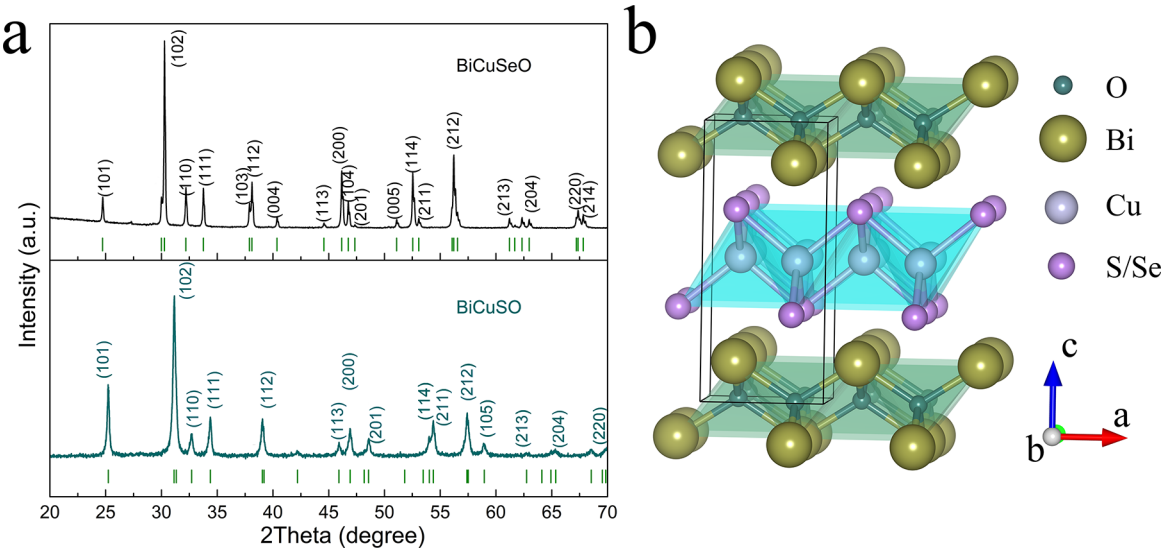

Figure 1. (a) Powder XRD patterns of as-prepared BiCuSO and BiCuSeO. (b) The crystal structure of BiCu*Ch*O with antifluorite OBi_4 tetrahedra and fluorite Cu*Ch*$_4$ tetrahedra stacking alternatively along the *c* axis. Cyan, brown, light violet, and purple spheres represent O^{2-}, Bi^{3+}, Cu^{+}, and Ch^{2-} ions, respectively. Light green and cyan polyhedra represent the edge-sharing Cu*Ch*$_4$ and OBi_4 tetrahedra.

strontium-doped samples to 1.5 for Ca and Pb dual-doped samples.[9,14] All aforementioned approaches aim to optimize the TE performance in terms of the structural stability, electronic structure, and related physical properties of BiCuSeO. In addition, Berardan et al. performed comprehensive studies on the structure and transport evolution of BiCu*Ch*O under different chemical pressures generated via chalcogen solid solution method.[15,16]

External pressure, as an alternative factor of temperature and chemical composition that can affect the structural and electronic properties of condensed matters, provides a unique method to explore new materials with tailored electrophysical properties.[17,18] Recently, Ma et al. reported an abnormal phase transition from sodium metal to an optically transparent high-pressure phase of sodium with a band gap of 1.3 eV at ∼200 GPa, which was attributed to the pressure-driven *p*−*d* hybridizations of the valence electrons and their repulsion by core electrons into the lattice interstices.[19] Likewise, in semiconductors, pressure often plays an important role on broadening the conduction band and valence band to enhance the electric transport performance. For example, in TiO_2 and Ta_2O_5, improved electrical conductivities compared with those of the raw materials were achieved via pressure-induced phase transitions and amorphization.[20,21] The layered semiconductor BiOCl was reported undergoing a tetragonal to tetragonal isostructural phase transition at 22.1 GPa, accompanied by the redistribution of Bader charge among the Bi, O, and Cl ions.[22] More comprehensive studies of semiconductors under high pressure are suggestive to the ambient chemical manipulations of Birich photocatalysts at ambient conditions.[23−26]

In this paper, oxychalcogenides BiCu*Ch*O (*Ch* = S, Se) are selected as representatives to study the pressure impact on 2D semiconductors. In situ characterizations including synchrotron X-ray diffraction, Raman spectra, and photocurrent and transport measurements were performed under high pressure. Meanwhile, we also discussed the origins of enhanced electric conductivity and better optoelectric properties with band theory from the competition between pressure-induced band gap opening and charge delocalization. Theoretical calculation was also applied to confirm the mechanism of the abnormal transport behavior of BiCuSeO observed experimentally under high pressure.

EXPERIMENTAL DETAILS

Sample Syntheses. BiCuSO and BiCuSeO polycrystals were synthesized by using a high-temperature high-pressure method followed by spark plasma sintering (SPS). First, high-purity Bi_2O_3 (powder, 99.999%), Bi (shot, 99.999%), S/Se (shot, 99.999%), and Cu (powder, 99.999%) in a stoichiometric ratio were mixed uniformly in an agate mortar. Then, the mixture was shaped into a cylinder with about 10.8 mm in diameter and 6 mm in height and loaded into a standard assembly cell made by graphite heater and *h*-BN crucible for high-pressure and high-temperature synthesis with the conditions of 1073 K and 3 GPa for 0.5 h. Finally, the prefabricated BiCu*Ch*O cylinders were ground into fine powders for the subsequent SPS sintering at 953 K and 60 MPa for 0.5 h, in order to generate homogeneously dense well-crystalline solids.

Structural Characterizations under High Pressure. In situ high-pressure angle-dispersive X-ray diffraction (XRD) measurements were performed with a synchrotron source at beamline 16 BM-D (λ = 0.3066 Å) and 13BM-C (λ = 0.434 Å)[27] of the Advanced Photon Source (APS), Argonne National Laboratory (ANL). A symmetric diamond anvil cell (DAC) with a 300 μm culet diameter was used to generate high pressure. Rhenium gaskets with holes that are 45 μm in thickness and 150 μm in diameter served as sample chambers. BiCu*Ch*O samples were ground into fine powders and then compacted and loaded into the sample chamber together with silicone oil as the pressure-transmitting medium. Pressure was measured and calibrated by using the ruby fluorescence method.[28] The 2D XRD patterns were integrated by using the Fit2D software[29] and refined with the Rietveld method using the General Structure Analysis System (GSAS) and graphical user interface EXPGUI package.[30] High-pressure Raman spectra were measured with a 633 nm laser of 1.73 mW power. It has been verified that the local heating effect from the laser during data acquisition can be neglected. Raman studies

DOI: 10.1021/acs.jpcc.8b04996
J. Phys. Chem. C 2018, 122, 15929−15936

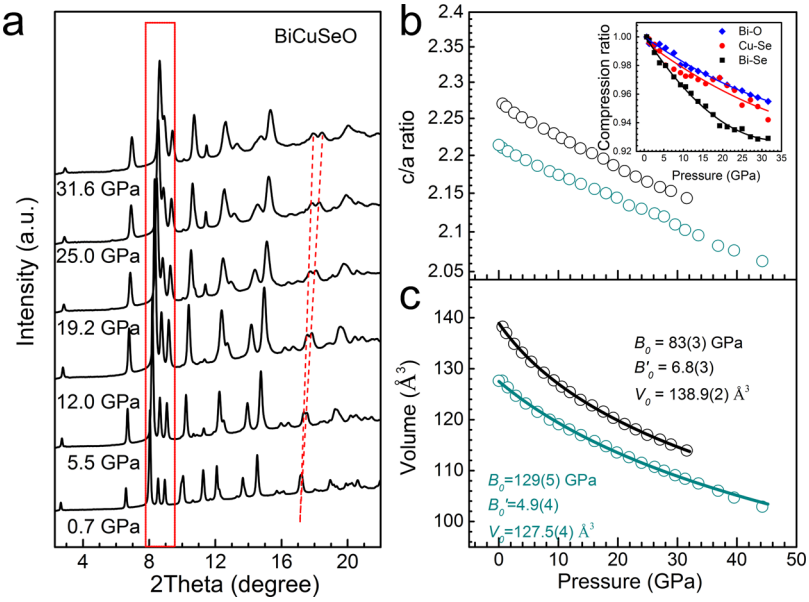

Figure 2. Selected angle-dispersive XRD patterns of (a) BiCuSeO under compression with an incident wavelength of 0.3066 Å at room temperature. (b) and (c) show the pressure dependence of *c*/*a* and volume (*V*) for BiCu*Ch*O. The bond lengths of BiCuSeO as a function of pressure are given in the inset of (b). The solid line in (c) shows the fitted third-order Birch−Murnaghan EOS.

were performed under the same sample conditions as the XRD measurements.

Transport Measurements under High Pressure. Electrical resistance measurements were carried out by using the four-probe resistance method. A thin cubic BN layer was inserted between the steel gasket and diamond anvils to insulate the metal gasket from the sample. Four platinum wires (2.5 μm in thickness) were arranged to contact the sample surface in the chamber. A Keithley 6221 current source, 2182A nanovoltmeter, and 7001 switch systems were used as the current supply, voltmeter, and voltage/current switcher, respectively. The resistivity was determined by the Van de Pauw method.[31] For the photocurrent measurements, the same sample setup was applied as the transport measurements. A 50 W incandescent lamp was used as the irradiation source (~5 mWcm^{-2} on the sample). The photo response was measured in the dark and under illumination at selected pressure points.

Theoretical Calculations. By relaxing the atomic structure, we performed the electronic structure simulation of BiCuSeO at different pressures using the density function theory (DFT) and projector augment wave method (PAW) as implemented in the Vienna ab initio Simulation Package (VASP).[32] The Perdew−Burke−Ernzerhof (PBE) was treated as the exchange-correlation potential within a generalized gradient approximation (GGA).[33] The cutoff energy of the plane wave was set to 600 eV, and a Monkhorst−Pack *k*-mesh of 31 × 31 × 13 was used to sample the Brillouin zone for integrations in reciprocal space. The energy convergence criterion was 10^{-6} eV per unit cell, and the force on all relaxed atoms was less than 0.03 eV/Å. The on-site Coulomb interactions (DFT+*U*) method was chosen to calculate the electronic structure. The effective Coulomb repulsion parameter *U* was set to 4 eV referring to the similar material systems.[34]

RESULTS AND DISCUSSION

The ambient XRD patterns of the as-prepared BiCuSeO are shown in Figure 1a. All of the peaks could be well assigned to the known tetragonal *P*4/*nmm* structure, and no secondary peaks were observed, indicating that phase-pure BiCu*Ch*O powders were fabricated successfully. The broader peaks for the sulfide than those of selenide here come from the different X-ray scanning conditions such as step size, dwelling time, and incident slits, rather than the extent of disorder of copper vacancies. This also can be validated by the later synchrotron XRD results, as collected from fine powders with submicron grain sizes. The refined lattice parameters are a = 3.867(2) Å and c = 8.546(5) Å for BiCuSO and a = 3.927(2) Å and c = 8.926(5) Å for BiCuSeO, which are close to those given in the literature.[35,36] The lattice constants of BiCuSeO raise a little for that the radius of sulfur is smaller than that of selenium. Both BiCuSeO and BiCuSO are built up of edge-sharing OBi_4 and $CuCh_4$ tetrahedra, which are alternatively stacked along the c axis, as shown in Figure 1b. It is considered that the equivalent substitution of selenium by sulfur takes place only in the $[Cu_2Ch_2]$ layer of the structure, which should not significantly influence the local structure of the $[Bi_2O_2]$ layers, and the Bi−O bond lengths should remain almost the same. The intralayer and the interlayer bond lengths are 2.329(2) Å and 2.303(2) Å for Bi−O and 3.24(3) Å and 3.205(3) Å for Bi−*Ch*, for the Se and S polymorphs, respectively, according to the Rietveld refinement results.

To investigate the structural stability and lattice evolution under high pressure, synchrotron XRD was performed on fine powders of BiCuSeO and BiCuSO. Figures 2a and S1 present the XRD patterns of BiCuSeO and BiCuSO as functions of pressure. Under compression, all of the diffraction peaks shifted to higher angles simultaneously, corroborating the volume compression. The original tetragonal structure was preserved to the highest pressure without any emerging new XRD peaks, implying the robust stability of the BiCu*Ch*O crystal structure. The broadening of the Bragg peaks under high pressure originate from the grain size reduction and the increased local stains between them as well as the non-hydrostatic pressure after high-pressure treatments, which has commonly been observed in high-pressure experiments. It is

DOI: 10.1021/acs.jpcc.8b04996
J. Phys. Chem. C 2018, 122, 15929−15936

worthy to note that the (102) and (110) peaks at around 9° (2θ) approach each other during compression and merged together eventually, owing to the larger pressure-induced shortening of the interlayer Bi−*Ch* bond lengths along the *c* axis (as shown in the inset of Figure 2b). While for the interlayer Bi−Se bonds, they show larger shrinkages than those of the intralayer bonds, such as Cu−Se and Bi−O bonds. Copper deficiency was not taken into consideration here, for it had little effect on the change of bonds (details are provided in Figure S2). Moreover, peaks located at around 17° indexed to (220), (106), (214), and (221) split up as pressure increased (Figure S3), instead of new peaks appearing, which is confirmed by the Rietveld refinement in Figure S4. All of the Rietveld refinement results can be found in Table S1 of the Supporting Information. Along with the decreased lattice parameter ratio (*c*/*a*) under compression, all of these clues indicate an anisotropic compressibility along different crystallographic axes, as shown in Figure 2b. These structural behaviors of BiCu*Ch*O are quite different from those of other similar 2D compounds such as NdOFeAs[37] and BiOCl,[22] in which isostructural phase transitions were observed under compression. The anisotropic compressibility of BiCu*Ch*O could be associated with the distinct electronic configurations in the alternative conductive and insulating layers.

To further elucidate this phenomenon, the equation of states (EOS) of BiCu*Ch*O were fitted using the third-order Birch−Murnaghan method[38] (as shown in Figure 2c)

$$P = \frac{3}{2}B_0\left[\left(\frac{V_0}{V}\right)^{7/3} - \left(\frac{V_0}{V}\right)^{5/3}\right] \times \left\{1 + \frac{3}{4}(B_0' - 4) \times \left[\left(\frac{V_0}{V}\right)^{3/2} - 1\right]\right\}$$

The bulk modulus B_0 values of 129(5) and 83(3) GPa under pressure, as well as the derivative B_0' of 4.9(4) and 6.8(3) for BiCuSO and BiCuSeO were determined, respectively. These values suggest an increased compressibility and a decreased elastic stiffness from *Ch* = Se to S. The fitted bulk modulus B_0 for BiCuSeO is close to the reported Young's modulus values of 76.5[36] and 78.8 GPa[39] and matches well with the first-principle calculation result of 75.2(5) GPa. The calculated value of the unit cell volume at ambient pressure V_0 is 138.9(2) Å^3, which is close to that (137.8 Å^3) obtained experimentally.

Raman spectroscopy was employed to characterize the pressure-induced local structure evolution of BiCu*Ch*O, which was considered sensitive to the subtle change of the vibration, rotation, and other low-frequency modes of materials. According to the group theory, there are in total eight Raman active modes in BiCu*Ch*O system: $\Gamma_{Raman} = 2A_{1g} + 2B_{1g} + 4E_g$.[40] At ambient conditions, only four Raman modes can be observed at 59.7, 88.0, 146.2, and 176.0 cm^{-1}, corresponding to E_g^1, E_g^2, A_{1g}^1, A_{1g}^2 (labeled as M1, M2, M3, and M4), respectively. The locations of the experimental Raman modes are consistent with the simulation results from DFT calculations.[41] The in-plane motion of Cu is involved in the two lower-frequency E_g Raman modes (~59.7 and 88.0 cm^{-1}). Bi and Se atoms in the tetrahedra are mainly involved in the A_{1g} modes due to the out-of-plane vibrations. With increasing pressure, the second A_{1g}^2 peak of BiCuSeO splits into two individual peaks at 18.3 GPa (as shown in Figure 3a). A similar change is also found in BiCuSO around 24 GPa for the second A_{1g} mode (152.7 cm^{-1}), as shown in Figure S5. These emerging M5 modes could be assigned to another E_g mode associated with the in-plane motion of Se and Bi. It is expected that the substitution of Se by S should evidently shift the

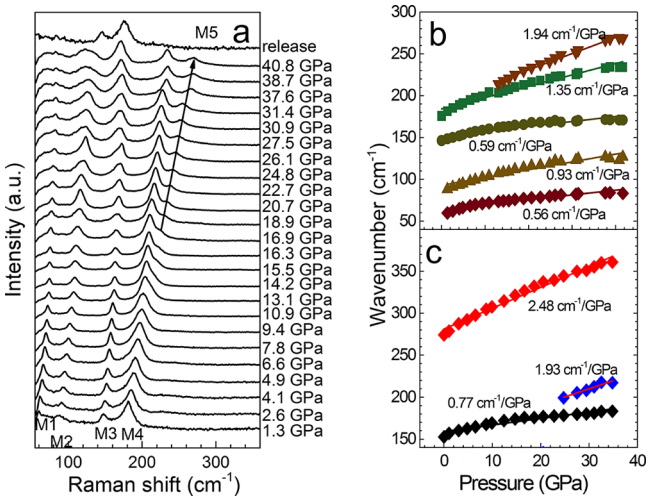

Figure 3. Raman spectra for (a) BiCuSeO at various pressures. (b,c) The pressure dependence of selected Raman peaks for BiCuSeO and BiCuSO.

second A_{1g} vibration mode from 176.0 to 152.7 cm^{-1} and reduce the third E_g vibration mode. Moreover, a high-frequency peak marked as M6 is observed in BiCuSO (as shown in Figure S5), which can be as assigned to the B_{1g} mode aroused from the motion of oxygen atoms. Under compression, all of the Raman peaks shift to higher wavenumbers because of the shrinking of bond lengths (as shown in Figure 3b). The shift coefficients under high pressure are calculated to be 0.56, 0.93, 0.59, 1.35, and 1.94 cm^{-1}/GPa for the M1−M5 modes of BiCuSeO, respectively, and 0.77, 1.93, and 2.48 cm^{-1}/GPa for M4−M6 modes of BiCuSO, respectively (Figure 3c). The experimental data exhibit coincident trends compared to previous simulations (1.08, 2.83, 4.48, 2.98, 4.62 cm^{-1}/GPa).[41] Upon decompression, all of the Raman peaks regress to their original positions, indicating a reversible structure change. All of these findings are in good agreement with our XRD results.

The electrical transport property is one of the key parameters for semiconductors especially in photovoltaic, optoelectronic, and thermoelectric applications. In order to evaluate the pressure impact on the transport properties of BiCu*Ch*O, in situ resistance measurements were conducted for BiCuSeO under pressure. We used the Van der Pauw method to determine the resistivity with the equation $\exp(-\pi R_1/R_s) + \exp(-\pi R_2/R_s) = 1$, where R_1 and R_2 are the two individual resistances measured by the four-point probe method, and R_s is the sample resistance. Considering the thickness *t* of 45 μm, the electrical resistivity was calculated as $\rho = R_S \times t$. The first electrical resistivity of 97.5 mΩ·cm at 1.3 GPa was recorded, which matches well with the resistivities reported at ambient conditions.[35,39] As shown in Figure 4a, the resistivity of BiCuSeO decreases with increasing pressure in the first stage (P < 12 GPa), which is associated with the broadening and eventual overlap of the valence and conduction bands (VB and CB) caused by the shortening of bond lengths.[19,20] Such pressure-induced electronic transport enhancements were frequently observed in other semiconductors.[20,21] Above 12 GPa, BiCuSeO exhibits an abnormal resistivity increasing under compression up to 30 GPa. Since there is no structural phase transition for BiCuSeO, the resistance upturn is supposed to the competition between the broadening of VB/

DOI: 10.1021/acs.jpcc.8b04996
J. Phys. Chem. C 2018, 122, 15929−15936

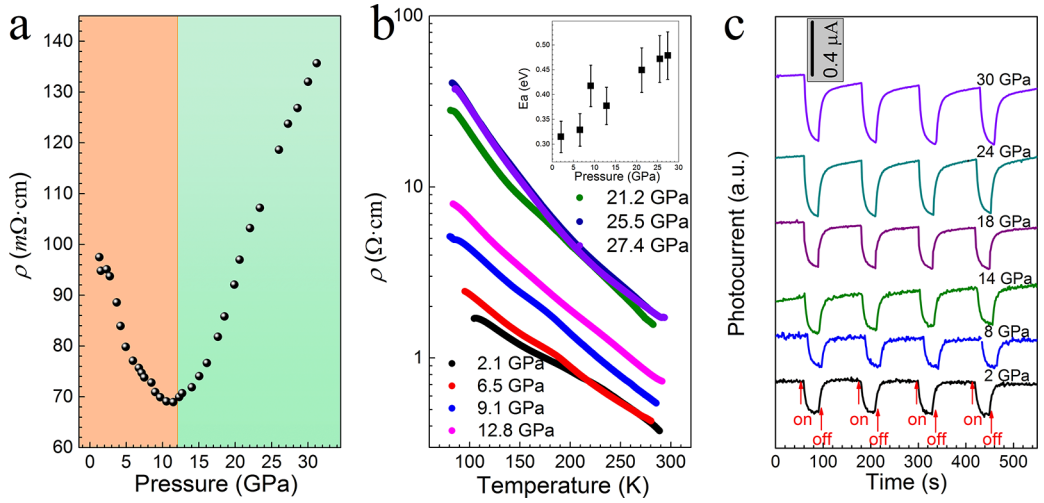

Figure 4. (a) Room temperature resistivity of BiCuSeO as a function of pressure. (b) The temperature dependence of resistivity at selected pressures. The inset shows the derived activation energy evolution as a function of pressure. (c) Photocurrent of BiCuSeO as a function of pressure.

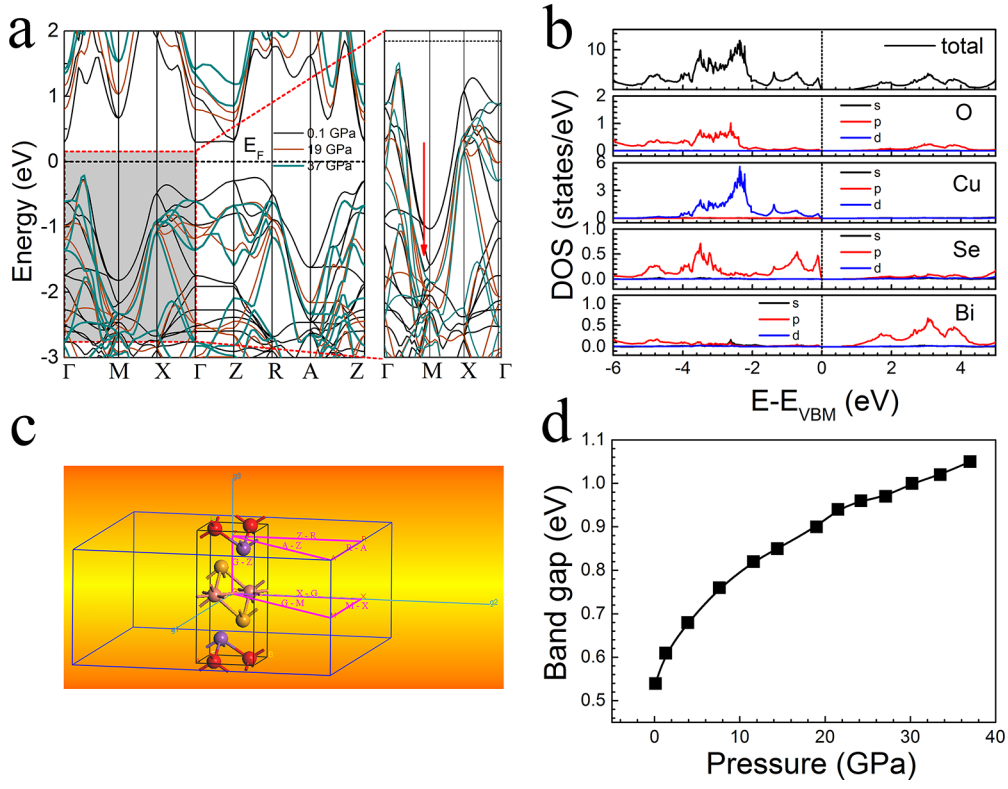

Figure 5. (a) Calculated band structure along high-symmetry directions at 0.1, 19, and 37 GPa. (b) Total and partial density of states at 0.1 GPa. (c) The Brillouin zone of BiCuSeO. (d) The calculated band gaps of BiCuSeO as a function of pressure.

CB and the band gap opening under compression. The former is dominant at low pressure, and the latter is responsible for the precipitous resistance increase at higher pressures.

The temperature dependence of the resistivity was also carried out for BiCuSeO at selected pressure points, as shown in Figure 4b. All of the data were collected during the slowly warming up stage from liquid nitrogen temperature (~80 K). BiCuSeO shows a typical semiconducting behavior in the pressure range of 0−30 GPa, since all of the resistivity curves decrease with increasing temperature. For an intrinsic semiconductor, the electronic conductivity is mainly from the contribution of thermally activated electrons jumping from the VB minimum to CB maximum. The conductivity in its Napierian logarithmic coordinate $\ln(\sigma)$ vs $1/T$ should follow the Arrhenius relationship and displays a linear trend: $\sigma = \sigma_0 \exp(E_a/k_B T)$, where σ_0, E_a, and k_B represents the pre-exponential constant, activation energy, and Boltzmann constant, respectively. The obtained activation energy E_a for BiCuSeO at various pressures by fitting the intrinsic T region above 200 K demonstrates a nearly linear increase of the band gaps with pressure, as shown in the inset of Figure 4b. The pressure-induced band gap opening indicated here could also be confirmed by the first-principle calculations and will be discussed later.

DOI: 10.1021/acs.jpcc.8b04996
J. Phys. Chem. C 2018, 122, 15929−15936

In situ photocurrent measurements were also conducted for BiCuSeO under high pressure. As shown in Figure 4c, a negative photocurrent response with light irradiation on indicates that the holes are the major carrier in this system. Actually, p-type conducting behavior of BiCuSeO is a normal case, since the copper vacancies will form unintentionally in the preparation process. The photocurrent is steady and reproducible during several intermittent on−off cycles. It is worth noting that the photocurrent improves continuously with increasing pressure and reaches almost twice enhancement at 30 GPa compared to that at the lowest pressure (Figure S6). The photocurrent enhancement indicates that either BiCuSeO has a higher separation rate of photoexcited electrons and holes from the VB to the CB under high pressure, or pressure plays a crucial role in inhibiting the recombination of electrons and holes because of its ability of engineering the electronic band structure. Our investigation results thus point out a new route other than chemical doping to improve the optoelectronics and may lead to the discoveries of more optoelectronic materials with improved properties.

Although bandgap opening is a common contributor of the resistivity increase, it is not the case in BiCuSeO when the pressure is below 12 GPa. To get further insight into the conducting behavior, the electronic structure at several pressures was calculated on the basis of the DFT implemented in the VASP package. Figure 5a,b describes the dispersion of energy bands and density of states (DOS) of BiCuSeO, while Figure 5c pictured the selected high-symmetry points at various hydrostatic pressures. At ambient pressure, BiCuSeO shows an indirect band gap feather as reported;[7,34] to be more specific, the CB maximum was located at the Z point, while the VB minimum exists along the Γ−M line. The calculated band gap of 0.54 eV for BiCuSeO at 0.1 GPa is quite close to the values previously presented (0.38 and 0.47 eV, simulated by employing PBE + U + SOC potential and PBE96 GGA functional, respectively).[7,34] A multiband structure featured with several hole pockets at degenerated directions of the M−X−Γ line is obvious in this study. These hole pockets determine the electrical conductivity of p-type BiCuSeO and become deeper with increasing pressure, leading to a better conduction behavior.[42] As shown in Figure 5b, the upper part of the VB of BiCuSeO at 0.1 GPa is mainly due to the hybridization between the Cu 3d and Se 4p orbitals in the Cu−Se antibonding states. The Cu−Se antibonding states become more hybridized as the result of the pressure-driven $CuSe_4$ tetrahedral shrinkage, which will lead to the resistivity drop in the pressure range below 12 GPa. On the other hand, the band gap increases monotonously with pressure from 0.54 eV at 0.1 GPa to 1.07 eV at 37 GPa (as shown in Figure 5d). One can infer that it is Cu−Se bond length shrinkage instead of $CuSe_4$ tetrahedral tilting that is responsible for the pressure-induced band gap opening. This unusual interplay between the crystal structure and the electronic structure has also been observed in other semiconductors such as lithium cobaltite oxides under hydrostatic pressure.[43] Future efforts on tailoring the electronic configuration of 2D semiconductors by employing external pressure will be expected to discover more intriguing phenomena and novel pressure-responsive functional materials.

CONCLUSIONS

In summary, we studied the pressure effects on the structural and electronic properties of layered semiconductors BiCu*Ch*O (*Ch* = S, Se). Their tetragonal crystal structure is robust up to 32.0 GPa without any symmetry change. An abnormal pressure-induced upturn in resistivity was observed around 12.0 GPa for BiCuSeO, which is associated with the competition between pressure-induced charge delocalization and band gap opening. Moreover, BiCuSeO exhibits a greatly enhanced photo responsibility under high pressure. These results provide an in-depth understanding of the interplays between lattice and electron in 2D semiconductors. This demonstration also provides a promising band structure engineering approach that may lead to better optoelectronic performance.

ASSOCIATED CONTENT

Supporting Information

The Supporting Information is available free of charge on the ACS Publications website at DOI: 10.1021/acs.jpcc.8b04996.

Angle-dispersive XRD patterns of BiCuSO under compression (Figure S1), bong-length evolution (Bi−O, Bu-Se, Bi−Se) under pressure for BiCuSeO (Figure S2), Bragg peak position evolution with pressure for BiCuSeO in the specified two-theta region from 17.0 to 18.9° (Figure S3), the graphic refinements and results of BiCuSeO (Figure S4 and Table S1), Raman spectra for BiCuSO at high pressures (Figure S5), as well as the photocurrent intensity variation with pressure (Figure S6) (PDF)

AUTHOR INFORMATION

Corresponding Authors

*E-mail: yangwg@hpstar.ac.cn (W.Y.)
*E-mail: yonggang.wang@hpstar.ac.cn (Y.W.)

ORCID

Yonggang Wang: 0000-0003-4816-9182
Wenge Yang: 0000-0002-1825-2826

Notes

The authors declare no competing financial interest.

ACKNOWLEDGMENTS

This work was financially supported by the National Nature Science Foundation of China (Grant No. 51527801 and 11774015), NSAF (Grant No. U1530402), and Science Challenge Project No. TZ2016001. HPCAT operations are supported by the DOE-NNSA under Award No. DE-NA0001974 and by the DOE-BES under Award No. DE-FG02-99ER45775, with partial instrumentation funding by NSF. GeoSoilEnviroCARS is supported by the National Science Foundation−Earth Sciences (EAR-1634415) and Department of Energy−GeoSciences (DE-FG02-94ER14466). The PX^2 program is supported by COMPRES under NSF Cooperative Agreement EAR-1661511. APS is supported by the DOE-BES, under Contract No. DE-AC02-06CH11357. The authors thank Y.S. Zhao, C. Xu (HPSTAR), and C. Kenney-Benson (HPCAT) for their valuable suggestions and technique support.

REFERENCES

(1) Kamihara, Y.; Hiramatsu, H.; Hirano, M.; Kawamura, R.; Yanagi, H.; Kamiya, T.; Hosono, H. Iron-Based Layered Superconductor: LaOFeP. *J. Am. Chem. Soc.* **2006**, *128* (31), 10012−10013.
(2) Watanabe, T.; Yanagi, H.; Kamiya, T.; Kamihara, Y.; Hiramatsu, H.; Hirano, M.; Hosono, H. Nickel-Based Oxyphosphide Super-

DOI: 10.1021/acs.jpcc.8b04996
J. Phys. Chem. C 2018, 122, 15929−15936

conductor with a Layered Crystal Structure, LaNiOP. *Inorg. Chem.* **2007**, *46* (19), 7719−7721.
(3) Kamihara, Y.; Watanabe, T.; Hirano, M.; Hosono, H. Iron-Based Layered Superconductor La[$O_{1-x}F_x$]FeAs (x = 0.05−0.12) with Tc = 26 K. *J. Am. Chem. Soc.* **2008**, *130* (11), 3296−3297.
(4) Ueda, K.; Inoue, S.; Hirose, S.; Kawazoe, H.; Hosono, H. Transparent P-type Semiconductor: LaCuOS Layered Oxysulfide. *Appl. Phys. Lett.* **2000**, *77* (17), 2701−2703.
(5) Ueda, K.; Inoue, S.; Hosono, H.; Sarukura, N.; Hirano, M. Room-Temperature Excitons in Wide-Gap Layered-Oxysulfide Semiconductor: LaCuOS. *Appl. Phys. Lett.* **2001**, *78* (16), 2333−2335.
(6) Kamioka, H.; Hiramatsu, H.; Hirano, M.; Ueda, K.; Kamiya, T.; Hosono, H. Excitonic Properties Related to Valence Band Levels Split by Spin−Orbit Interaction in Layered Oxychalcogenide LaCuO*Ch*(*Ch*=S,Se). *J. Lumin.* **2005**, *112* (1), 66−70.
(7) Hiramatsu, H.; Yanagi, H.; Kamiya, T.; Ueda, K.; Hirano, M.; Hosono, H. Crystal Structures, Optoelectronic Properties, and Electronic Structures of Layered Oxychalcogenides *M*CuO*Ch* (*M* = Bi, La; *Ch* = S, Se, Te): Effects of Electronic Configurations of M^{3+} Ions. *Chem. Mater.* **2008**, *20* (1), 326−334.
(8) Liu, Y.; Zhao, L. D.; Liu, Y.; Lan, J.; Xu, W.; Li, F.; Zhang, B. P.; Berardan, D.; Dragoe, N.; Lin, Y. H.; et al. Remarkable Enhancement in Thermoelectric Performance of BiCuSeO by Cu Deficiencies. *J. Am. Chem. Soc.* **2011**, *133* (50), 20112−20115.
(9) Liu, Y.; Zhao, L. D.; Zhu, Y.; Liu, Y.; Li, F.; Yu, M.; Liu, D. B.; Xu, W.; Lin, Y. H.; Nan, C. W. Synergistically Optimizing Electrical and Thermal Transport Properties of BiCuSeO via a Dual-Doping Approach. *Adv. Energy Mater.* **2016**, *6* (9), 1502423.
(10) Pei, Y. L.; Wu, H.; Wu, D.; Zheng, F.; He, J. High Thermoelectric Performance Realized in a BiCuSeO System by Improving Carrier Mobility through 3D Modulation Doping. *J. Am. Chem. Soc.* **2014**, *136* (39), 13902−8.
(11) Lan, J. L.; Liu, Y. C.; Zhan, B.; Lin, Y. H.; Zhang, B.; Yuan, X.; Zhang, W.; Xu, W.; Nan, C. W. Enhanced Thermoelectric Properties of Pb-Doped BiCuSeO Ceramics. *Adv. Mater.* **2013**, *25* (36), 5086−90.
(12) Liu, Y.; Ding, J.; Xu, B.; Lan, J.; Zheng, Y.; Zhan, B.; Zhang, B.; Lin, Y.; Nan, C. Enhanced Thermoelectric Performance of La-doped BiCuSeO by Tuning Band Structure. *Appl. Phys. Lett.* **2015**, *106* (23), 233903.
(13) Sui, J.; Li, J.; He, J.; Pei, Y. L.; Berardan, D.; Wu, H.; Dragoe, N.; Cai, W.; Zhao, L. D. Texturation Boosts the Thermoelectric Performance of BiCuSeO Oxyselenides. *Energy Environ. Sci.* **2013**, *6* (10), 2916.
(14) Zhao, L. D.; Berardan, D.; Pei, Y. L.; Byl, C.; Pinsard-Gaudart, L.; Dragoe, N. $Bi_{1-x}Sr_xCuSeO$ Oxyselenides as Promising Thermoelectric Materials. *Appl. Phys. Lett.* **2010**, *97* (9), 092118.
(15) Barreteau, C.; Pan, L.; Amzallag, E.; Zhao, L. D.; Bérardan, D.; Dragoe, N. Layered Oxychalcogenide in the Bi−Cu−O−Se System as Good Thermoelectric Materials. *Semicond. Sci. Technol.* **2014**, *29* (6), 064001.
(16) Berardan, D.; Li, J.; Amzallag, E.; Mitra, S.; Sui, J.; Cai, W.; Dragoe, N. Structure and Transport Properties of the BiCuSeO-BiCuSO Solid Solution. *Materials* **2015**, *8* (3), 1043−1058.
(17) Sun, L.; Chen, X. J.; Guo, J.; Gao, P.; Huang, Q. Z.; Wang, H.; Fang, M.; Chen, X.; Chen, G.; Wu, Q.; et al. Re-Emerging Superconductivity at 48 K in Iron Chalcogenides. *Nature* **2012**, *483* (7387), 67−9.
(18) Zhang, G.; Liu, F.; Gu, T.; Zhao, Y.; Li, N.; Yang, W.; Feng, S. Enhanced Ferroelectric and Visible-Light Photoelectric Properties in Multiferroic $KBiFe_2O_5$ via Pressure-Induced Phase Transition. *Adv. Electron. Mater.* **2017**, *3* (3), 1600498.
(19) Ma, Y.; Eremets, M.; Oganov, A. R.; Xie, Y.; Trojan, I.; Medvedev, S.; Lyakhov, A. O.; Valle, M.; Prakapenka, V. Transparent Dense Sodium. *Nature* **2009**, *458* (7235), 182−5.
(20) Lu, X.; Hu, Q.; Yang, W.; Bai, L.; Sheng, H.; Wang, L.; Huang, F.; Wen, J.; Miller, D. J.; Zhao, Y. Pressure-iInduced Amorphization in Single-crystal Ta_2O_5 Nanowires: a Kinetic Mechanism and Improved Electrical Conductivity. *J. Am. Chem. Soc.* **2013**, *135* (37), 13947−53.
(21) Lu, X.; Yang, W.; Quan, Z.; Lin, T.; Bai, L.; Wang, L.; Huang, F.; Zhao, Y. Enhanced Electron Transport in Nb-doped TiO_2 Nanoparticles via Pressure-Induced Phase Transitions. *J. Am. Chem. Soc.* **2014**, *136* (1), 419−26.
(22) Zhao, J.; Xu, L.; Liu, Y.; Yu, Z.; Li, C.; Wang, Y.; Liu, Z. Isostructural Phase Transition in Bismuth Oxide Chloride Induced by Redistribution of Charge under High Pressure. *J. Phys. Chem. C* **2015**, *119* (49), 27657−27665.
(23) Ye, L.; Su, Y.; Jin, X.; Xie, H.; Zhang, C. Recent advances in BiO*X* (*X* = Cl, Br and I) Photocatalysts: Synthesis, Modification, Facet Effects and Mechanisms. *Environ. Sci.: Nano* **2014**, *1* (2), 90.
(24) Kunioku, H.; Nakada, A.; Higashi, M.; Tomita, O.; Kageyama, H.; Abe, R. Improved Water Oxidation under Visible Light on Oxyhalide Bi_4MO_8X (*M* = Nb, Ta; *X* = Cl, Br) Photocatalysts Prepared Using Excess Halogen Precursors. *Sustainable Energy Fuels* **2018**, *2*, 1474.
(25) Zeng, C.; Hu, Y.; Huang, H. $BiOBr_{0.75}I_{0.25}/BiOIO_3$ as A Novel Heterojunctional Photocatalyst with Superior Visible-light-driven Photocatalytic Activity in Removing Diverse Industrial Pollutants. *ACS Sustainable Chem. Eng.* **2017**, *5* (5), 3897−3905.
(26) Feng, J.; Huang, H.; Yu, S.; Dong, F.; Zhang, Y. A Self-sacrifice Template Route to Iodine Modified $BiOIO_3$: Band Gap Engineering and Highly Boosted Visible-light Active Photoreactivity. *Phys. Chem. Chem. Phys.* **2016**, *18* (11), 7851−7859.
(27) Zhang, D.; Dera, P. K.; Eng, P. J.; Stubbs, J. E.; Zhang, J. S.; Prakapenka, V. B.; Rivers, M. L. High Pressure Single Crystal Diffraction at PX̂2. *J. Visualized Exp.* **2017**, No. 119, 54660.
(28) Mao, H. K.; Xu, J.; Bell, P. M. Calibration of the Ruby Pressure Gauge to 800 kbar under Quasi-Hydrostatic Conditions. *J. Geophys. Res.* **1986**, *91* (B5), 4673−4676.
(29) Hammersley, A. P.; Svensson, S. O.; Hanfland, M.; Fitch, A. N.; Hausermann, D. Two-Dimensional Detector Software: From Real Detector to Idealised Image or Two-Theta Scan. *High Pressure Res.* **1996**, *14* (4−6), 235−248.
(30) Larson, A. C.; Von Dreele, R. B. *GSAS General Structure Analysis System*; Report LAUR 86−748; Los Alamos National Laboratory: Los Alamos, NM, USA, 2004.
(31) van der Pauw, L. J. A Method of Measuring Specific Resistivity and Hall Effect of Discs of Arbitrary Shape. *Philips Res. Rep* **1958**, *13*, 1−9.
(32) Kresse, G.; Furthmüller, J. Efficient Iterative Schemes for ab Initio Total-Energy Calculations Using a Plane-Wave Basis Set. *Phys. Rev. B: Condens. Matter Mater. Phys.* **1996**, *54* (16), 11169−11186.
(33) Perdew, J. P.; Burke, K.; Ernzerhof, M. Generalized Gradient Approximation Made Simple. *Phys. Rev. Lett.* **1996**, *77* (18), 3865−3868.
(34) Zou, D.; Xie, S.; Liu, Y.; Lin, J.; Li, J. Electronic Structures and Thermoelectric Properties of Layered BiCuO*Ch* Oxychalcogenides (*Ch* = S, Se and Te): First-principles Calculations. *J. Mater. Chem. A* **2013**, *1* (31), 8888.
(35) Barreteau, C.; Bérardan, D.; Zhao, L.; Dragoe, N. Influence of Te Substitution on the Structural and Electronic Properties of Thermoelectric BiCuSeO. *J. Mater. Chem. A* **2013**, *1* (8), 2921.
(36) Zhao, L. D.; He, J.; Berardan, D.; Lin, Y.; Li, J. F.; Nan, C. W.; Dragoe, N. BiCuSeO Oxyselenides: New Promising Thermoelectric Materials. *Energy Environ. Sci.* **2014**, *7* (9), 2900.
(37) Zhao, J.; Wang, L.; Dong, D.; Liu, Z.; Liu, H.; Chen, G.; Wu, D.; Luo, J.; Wang, N.; Yu, Y.; et al. Struture Stability and Compressibility of Iron-Based Superconductor Nd($O_{0.88}F_{0.12}$)FeAs under High Pressure. *J. Am. Chem. Soc.* **2008**, *130* (42), 13828−9.
(38) Birch, F. Finite Strain Isotherm and Velocities for Single-Crystal and Polycrystalline NaCl at High Pressures and 300 K. *J. Geophys. Res.* **1978**, *83* (B3), 1257−1268.
(39) Li, F.; Li, J. F.; Zhao, L. D.; Xiang, K.; Liu, Y.; Zhang, B. P.; Lin, Y. H.; Nan, C. W.; Zhu, H. M. Polycrystalline BiCuSeO Oxide as a Potential Thermoelectric Material. *Energy Environ. Sci.* **2012**, *5* (5), 7188.

DOI: 10.1021/acs.jpcc.8b04996
J. Phys. Chem. C 2018, 122, 15929−15936

(40) Hadjiev, V. G.; Iliev, M. N.; Sasmal, K.; Sun, Y. Y.; Chu, C. W. Raman Spectroscopy of *R*FeAsO(*R*=Sm, La). *Phys. Rev. B: Condens. Matter Mater. Phys.* **2008**, *77* (22), 220505.
(41) Saha, S. K. Exploring The Origin of Ultralow Thermal Conductivity in Layered BiOCuSe. *Phys. Rev. B: Condens. Matter Mater. Phys.* **2015**, *92* (4), 041202.
(42) Zou, D.; Liu, Y.; Xie, S.; Lin, J.; Zheng, H.; Li, J. High Pressure Effect on the Electronic Structure and Thermoelectric Properties of BiCuSeO: First-Principles Calculations. *RSC Adv.* **2014**, *4* (97), 54819−54825.
(43) Xu, C.; Xiao, W.; Liu, T.; Sun, F.; Zheng, J.; Peng, S.; Liu, X.; Pan, F.; Yang, W.; Mao, H. K. Pressure-Induced Abnormal Insulating State in Triangular Layered Cobaltite Li_xCoO_2 (x = 0.9). *J. Mater. Chem. A* **2017**, *5* (36), 19390−19397.

DOI: 10.1021/acs.jpcc.8b04996
J. Phys. Chem. C 2018, 122, 15929−15936